Structure, Vol. 12, 2015–2024, November, 2004, ©2004 Elsevier Ltd. All rights reserved. DOI 10.1016/j.str.2004.08.010

Structures of *Selenomonas ruminantium* Phytase in Complex with Persulfated Phytate: DSP Phytase Fold and Mechanism for Sequential Substrate Hydrolysis

Hsing-Mao Chu,[1,2,3,7] Rey-Ting Guo,[1,2,3,5,7] Ting-Wan Lin,[2] Chia-Cheng Chou,[2,3] Hui-Lin Shr,[2,3] Hui-Lin Lai,[4] Tsung-Yin Tang,[4] Kuo-Joan Cheng,[4] Brent L. Selinger,[6] and Andrew H.-J. Wang[1,2,3,5,*]

[1]Institute of Biochemical Sciences
National Taiwan University
Taipei 106
Taiwan
[2]Institute of Biological Chemistry
[3]Core Facility for Protein X-Ray Crystallography
[4]Institute of BioAgricultural Sciences
[5]Taiwan International Graduate Program
Academia Sinica
Taipei 115
Taiwan
[6]Department of Biological Sciences
University of Lethbridge
Lethbridge, Alberta
Canada

Summary

Various inositide phosphatases participate in the regulation of inositol polyphosphate signaling molecules. Plant phytases are phosphatases that hydrolyze phytate to less-phosphorylated *myo*-inositol derivatives and phosphate. The phytase from *Selenomonas ruminantium* shares no sequence homology with other microbial phytases. Its crystal structure revealed a phytase fold of the dual-specificity phosphatase type. The active site is located near a conserved cysteine-containing (Cys241) P loop. We also solved two other crystal forms in which an inhibitor, *myo*-inositol hexasulfate, is cocrystallized with the enzyme. In the "standby" and the "inhibited" crystal forms, the inhibitor is bound, respectively, in a pocket slightly away from Cys241 and at the substrate binding site where the phosphate group to be hydrolyzed is held close to the −SH group of Cys241. Our structural and mutagenesis studies allow us to visualize the way in which the P loop-containing phytase attracts and hydrolyzes the substrate (phytate) sequentially.

Introduction

Inositol polyphosphates (IPP) play important roles in a broad scope of cellular processes (Michell, 2002; Shamsuddin, 1999; Streb et al., 1983). Many inositide phosphatases participate in the regulation of these IPP signaling molecules, e.g., 5-phosphatases (Mitchell et al., 2002), 1-phosphatases (York et al., 1994), and 3-phosphatases (Lee et al., 1999). In plants, inositol hexakisphosphate [InsP(6)], often called phytate, is found in abundance in seeds, serving as an inorganic phosphate reservoir (Liu et al., 1998). Phytases are phosphatases that hydrolyze phytate to less-phosphorylated *myo*-inositol derivatives and inorganic phosphate. Recently, phytate has been found to promote dynamin I-mediated endocytosis (Hoy et al., 2002). Phytase activity also exists in human, and the enzyme appears to belong to the histidine phosphatase family (Caffrey et al., 1999).

Phytases are important enzymes in agricultural and animal applications. While phytases from various organisms may be used as additives, not all phytases are suitable sources. The phytase isolated from *S. ruminantium*, which is a bacterium living in the anaerobic rumen of ruminants, may be a good candidate for this purpose. This enzyme has been preliminarily characterized (Yanke et al., 1999) and shown to have excellent activity. To improve the properties for its applications, we sought to determine the three-dimensional structure, which is to be used as the basis for enzyme-engineering studies.

The crystal structures of three microbial phytases have been solved recently, revealing two types of protein folding. The first type, adopted by *Escherichia coli* and *Asperigerius niger,* has an α domain and a conserved α/β domain with two helices on each side of the seven-stranded sheet (Lim et al., 2000; Kostrewa et al., 1997). This type of enzyme contains a catalytic histidine in the conserved Arg-His-Gly motif to perform the nucleophilic attack, resulting in a phospho-histidine intermediate. These structures closely resemble the overall fold of other histidine acid phosphatases (Lim et al., 2000). The other type is the calcium-dependent phytase from *Bacillus amyloliquefaciens*, which adopts a β propeller conformation with six-stranded blades (Ha et al., 2000). The enzyme reaction appears to act through a direct attack of the metal-bridging water molecule on the phosphorous atom of phytate and the subsequent stabilization of the pentavalent transition state by the bound calcium ions. In contrast, *S. ruminantium* phytase neither contains the conserved Arg-His-Gly motif nor is affected by divalent metal ions. Surprisingly, the activity was nearly completely abolished by Fe^{2+}, Fe^{3+}, and Hg^{2+} ions and significantly retarded by Zn^{2+} ion (Yanke et al., 1999). These results suggested that the *S. ruminantium* phytase is likely to have a different phosphatase mechanism from that of the above mentioned phosphatases.

Herein, we report a third fold of phytase from *S. ruminantium* similar to the conserved fold of dual-specificity phosphatases. Structural studies of *S. ruminantium* phytase from three different crystal forms provide a plausible mechanism for the sequential hydrolysis of phytate by this novel P loop-containing phosphatase. In addition, results from the mutagensis of several catalytically important amino acids support the proposed mechanism.

Results and Discussion

Overall Structure of *S. ruminantium* Phytase

We have determined three different structures of the *S. ruminantium* phytase from three crystal forms: phytase alone (apo form), phytase bound with the IHS at a

*Correspondence: ahjwang@gate.sinica.edu.tw
[7]These authors contributed equally to this work.

Table 1. Data Collection and Refinement Statistics

Data Collection	Se-Met	Nat + IHS[d] Complex	Se-Met + IHS[d] Complex
Wavelength (Å)	0.9797	1.0710	1.0362
Space group	$P2_1$ (apo form)	$P2_12_12$ (inhibited form)	$C222_1$ (standby form)
Cell constants, *a*, *b*, *c* (Å)	46.47, 140.38, 80.68	161.30, 101.92, 46.06	128.38, 228.75, 91.78
Z[a]	2	2	3
Resolution (Å)/Completeness	2.0/93.2 (84.0)	2.5/98.8 (97.8)	2.5/84.0 (69.9)
Measurements/unique reflections	200,391/63,129	130,861/27,016	155,161/42,532
Average I/σ (I)/R_{merge} (%)	11.6/8.5	20.0/8.1	13.0/7.8
Refinement Statistics			
Reflections[b]	99,831 (1198)	44,488 (829)	37,388 (698)
R/R_{free} (%)[c]	18.0/22.1	20.7/26.0	17.9/26.5
Protein atoms/water atoms	5,114/1,312	5,107/675	7,606/951
IHS atoms[d]	—	3×36	2.5×36
Rms deviation for bond lengths (Å)	0.015	0.007	0.017
Rms deviation for bond angles (°)	1.68	1.33	1.98
Average B factor (Å^2)			
Main chain/side chain	18.4/27.6	32.1/33.3	29.2/30.7
Solvent/IHS[d]	39.3/—	37.7/83.1	33.5/58.9

Values in parentheses indicate the specific values in the highest resolution shell.
[a] Z, number of phytases in the asymmetric unit.
[b] Reflections, $I > 2\sigma$.
[c] R_{free} = R factor calculated using 5.0% of the reflection data chosen randomly and omitted from the start of refinement.
[d] IHS, *myo*-inositol hexasulfate.

location slightly away from the active site (standby form), and phytase bound with the IHS at the active site (inhibited form). The crystal structure of the apo form (to 2.0 Å resolution) was solved using the Se-Met enzyme by the single-wavelength anomalous diffraction method, while the other crystal structures of the standby and inhibited forms (to 2.5 Å resolution) were determined by the molecular replacement method. The detailed crystallographic information is listed in Table 1. The current model contains residues 23–336 with clear electron density. Figures 1B and 1C show the ribbon and surface diagrams of the complexes, respectively.

The structure of the phytase consists of two domains. The large domain has a protein fold in which a slightly twisted five-stranded β sheet (β2, β3, β11, β4, and β10) is sandwiched by two helices (αB and αD) on one side and three helices (αE, αF, and αG) on the other side. Two additional helices, a long αH helix (aa 290–315) and helix αI (aa 324–334) near the C-terminal end, lie near the edge of the large domain, forming the wall of a shallow pocket to support the binding of the substrate. Two loops, the first loop from aa 240–246 (called the P loop) and the second loop from aa 210–218 (called the WPD loop according to the protein tyrosine phosphatase 1B [PTP1B] nomenclature [Lohse et al., 1997]), provide the support from the bottom of the active-site pocket. The P loop contains the catalytically important $H_{240}C_{241}$XXGXXR(T/S) sequence motif. The small domain, enclosed within a box in Figure 1B, contains a five-stranded β barrel (β8, β7, β1, β6, and β5) in addition to a short β strand (β9) in the corner. Moreover, helix αC is located on the edge of the small domain. The *S. ruminantium* phytase adopts a football-like shape with the negatively charged IHS being buried in the active-site cavity, rimmed by positively charged Arg46, Arg57, Lys71, Lys72, His74, Lys176, Lys286, and Lys288 (Figure 1C).

The *S. ruminantium* phytase displays no structural similarity to the *E. coli* and *B. amyloliquefaciens* phytases. A search using DALI (Holm and Sander, 1998) showed substantial similarities between a portion of *S. ruminantium* phytase and the catalytic domain of the members of the cysteine phosphatase superfamily (Figure 1A), including LAR (Nam et al., 1999), KAPt (Song et al., 2001), and PTEN (Lee et al., 1999).

Active-Site Pocket

The active-site sequence (HCEAGVGR) of the phytase forms a loop (P loop) at the base of a substrate binding pocket that is characteristic of PTPs. The depth of this pocket is an important determinant of the substrate specificity of PTPs (Denu and Dixon, 1998). Especially for the phosphoinositide phosphatase PTEN, the wilder opening is necessary to accommodate the larger, phosphorylated inositol group of its substrate (Lee et al., 1999). Consistent with this suggestion, the phytase, in order to bind the fully phosphorylated inositol group, has a pocket ~14 Å deep with an opening of $\sim 6 \times 14$ Å, significantly deeper and wider than that of PTPs and PTEN. This difference is mainly due to the insertion of the small β domain and an extended helix αH compared to other PTPs.

Inhibitor Binding to the Basic Surface: Complex of the Standby Form

In the $C222_1$ (standby) form, the inhibitor in the complex has many interactions with the positive surface of the phytase. The IHS adopts two slightly different orientations (derived from two independent enzyme-inhibitor complexes in an asymmetric unit) (Figures 2A and 2B). The positive surface in the phytase, also present in other PTPs (Changela et al., 2001), is located at the interface between the two structural domains. It is composed of several loops (β7-β8 loop, β2-αA loop, conserved P

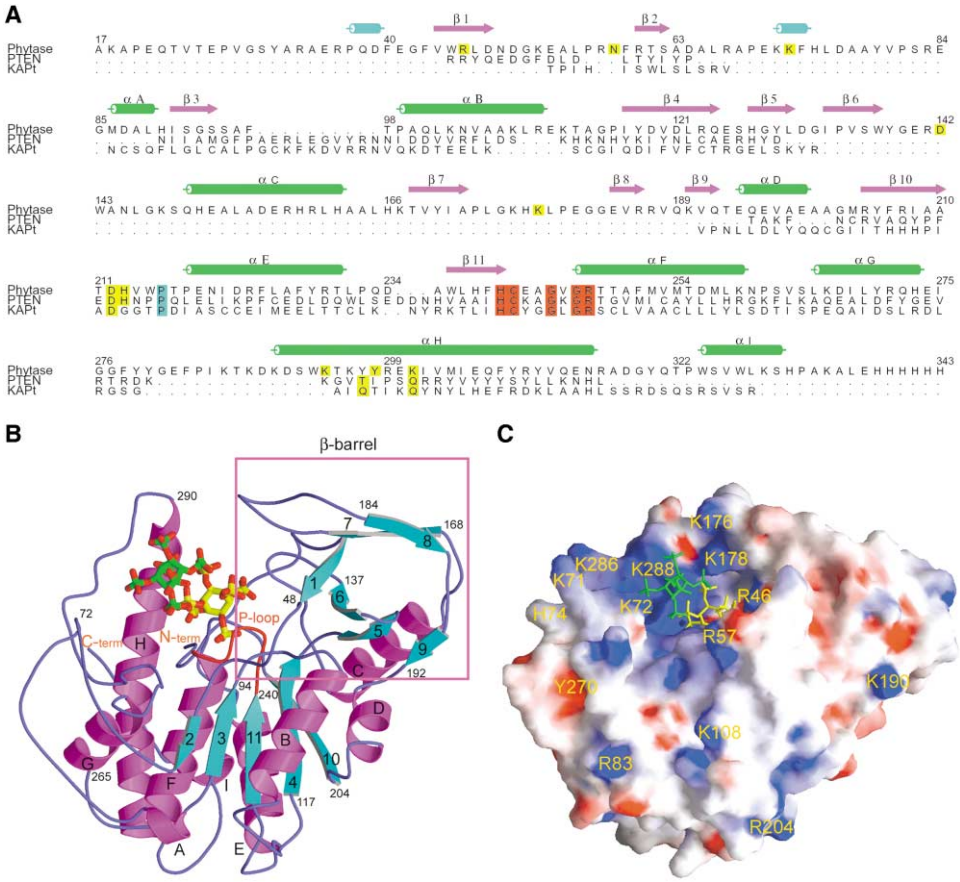

Figure 1. Overall Structure of *S. ruminantium* Phytase

(A) Structure-based amino acid sequence alignment of the *S. ruminantium* phytase with human PTEN and human KAPt, two members of the cysteine phosphatases. The alignment of the phosphatase domain, obtained with the program SPDBY (Guex and Peitsch, 1997), shows no apparent similarity of sequences outside the regions of conserved P loop (240–246) and WPD loop (between β10 and αE). Identical residues in the P loop are highlighted in red, while active-site amino acid residues are colored yellow, and an identical residue proline within all dual-specificity phosphatases is colored blue.

(B) View of enzyme with bound sulfated phytate at the active site (inhibited form in yellow) and location slightly away from the active site (standby form in green). The structure of the phytase consists of two domains, a large domain and a small domain. The small domain is indicated with a magenta box.

(C) A GRASP (Nicholls et al., 1991) electrostatic surface representation of the substrate binding pocket of *S. ruminantium* phytase with potentials ranging from −10 V (red) to +10 V (blue). A green and yellow stick model of the sulfated-phytate is shown in the broad and shallow binding pocket.

loop, and WPD loop), strand β7, and helix αH. A cluster of positively charged residues surrounding the active site form the inositol polyphosphate binding site and contribute to the reorientation of substrate in the sequential catalysis of phytase. The detailed interactions of the phytase in the standby form are shown in Figures 2C, 3A, and 3B.

Complex of the Inhibited Form

In the inhibited form of the complex, the active-site IHS was bound to the P loop using its 5-sulfate, making six hydrogen bonds with the amide NH groups and one hydrogen bond with the side chain of Arg247 from the HCXXGXXR motif (Figures 2D and 3C). Those contacts are similar to those found in other PTPs and DSPs (Denu et al., 1996). The interacting mode of the dipole of helix (αF) with the 5-sulfate was also found to exist in other histidine phosphatases such as *E. coli* phytase (11). The position and orientation of the conserved residues in the signature motif of PTP1B, KAPt, and PTEN are highly conserved and essential for catalysis. The Cβ atom of Ala243 and the Cγ atom of Val245 of nonconserved residues in the P loop are observed to be within van der Waals contacts of S1 and S3 of IHS. Besides the amide NH of P loop, Arg247 also plays a critical role in the binding of phytate. The Arg247 forms salt bridges with the carboxyl group of Glu125 (data not shown). Those interactions are conserved in both KAPt and PTP1B but absent in PTEN.

Arg247 plays an important role in the binding of both the carbonyl oxygen atom of Ala210 of the WPD loop and the sulfate group of the sulfated phytate. Asp142, which is usually not conserved in PTP, is located adjacent to the conserved Asp212 (Figure 2D). Asp142 might play a role in stabilizing the deprotonated Asp212, which is conserved among almost all PTPs, acting as a general acid to facilitate protonation to the scissile bond oxygen (Kim et al., 2001). It is in an identical position to the

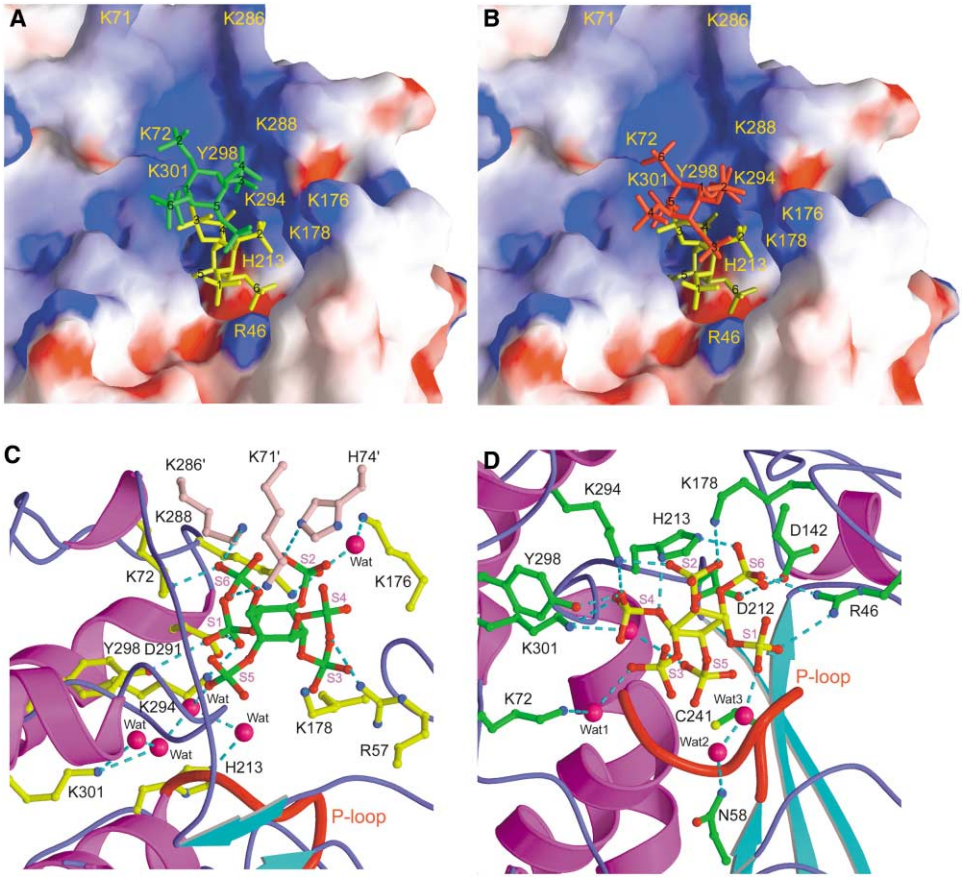

Figure 2. Overall Binding Mode of Sulfated Phytate with *S. ruminantium* Phytase

(A and B) An enlarged surface view of the active site with the IHS inhibitor bound in the inhibited location (IHS shown in yellow) and in the standby location (IHS shown in green and in red) for the two orientations found in the independent phytase enzymes in (B).

(C) Details of the interactions between the standby form IHS (the green one in [A]) and *S. ruminantium* phytase. The contact residues from the bound phytase are shown in yellow, and those from the neighboring phytase are shown in pink. The bound water molecules are represented as red spheres.

(D) Details of the interactions between the inhibited-form IHS and *S. ruminantium* phytase. Note that there are extensive hydrogen bonds between the P loop and the scissle phosphate (sulfate in IHS) group.

corresponding conserved Asp of PTEN (Asp92) and KAPt (Asp110). In addition to Asp212, another conserved His213 from the WPD loop forms two hydrogen bonds with the oxygen atoms of S6 and S4. Lys294, Tyr298, and Lys301 in helix αH also contribute multiple hydrogen bonds with several sulfate groups of IHS. Three well-ordered waters are present near the active site. These interactions suggest that the phytase binds and hydrolyzes the phosphate ester with a mechanism similar to that of PTP1B (Lohse et al., 1997).

Conformational Changes upon Substrate Binding

The conformation of the P loop in the inhibited form is similar to the P loop of PTEN and KAPt (Figure 5A). The P loop adopts two conformations, "open" in the apo form and "closed" in both standby and inhibited forms (Figure 5C). In order to form eight hydrogen bonds between the three oxygen atoms of 5-sulfate and the P loop signature motif, the ϕ/ψ dihedral angles of Gly244 changed from 98.4°/−160.4° in the open form to 65.0°/26.6° in the closed form. The Cα atom of Gly244 moves 4.21 Å with an accompanying 1.25 Å shift of the neighboring Cα atom of Ala243, resulting in the P loop adopting the closed conformation. The P loop of the standby form has no direct contact with the inhibitor, but the P loop adopts the same closed conformation as in the inhibited-form binding. Although the distance of the inhibitor to Cys241 of P loop is 8.56 Å in the standby form, the distant inhibitor still induced the P loop to form the closed conformation. Functionally, it may be advantageous to keep a closed conformation for the sequential dephosphorylation.

A small conformational change in phytase also occurs in the WPD loop, especially that associated with His213. His213 is thus located between two sulfate groups (S4 and S6) of the inhibitor to form two hydrogen bonds. Meanwhile, the position of carboxylic group of Asp212 is shifted. His213 of the WPD loop exists in many phosphoinositide phosphatases, such as PTEN, TPIP (Walker et al., 2001), and TPTE (Guipponi et al., 2001), but is absent in most general tyrosine phosphatases. The structure of the phytase-inhibitor complex suggests that His213 is important for specific binding to substrate and provides a precise positioning of Asp212.

Mutational Analysis

In order to correlate the function and structure of phytase, we have performed mutagenesis studies and fo-

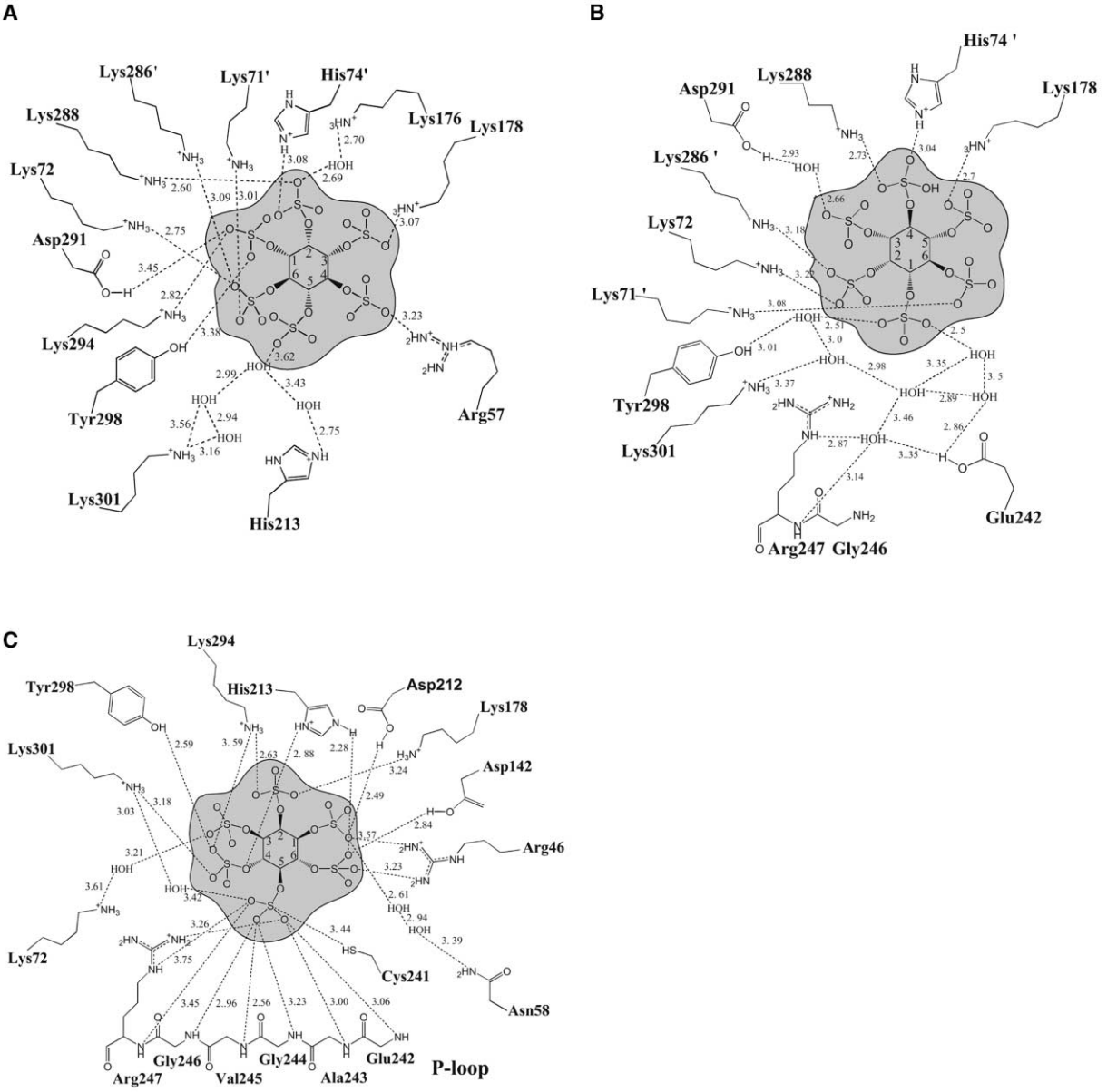

Figure 3. Schematic Diagrams of the Interactions Involved in IHS Binding

Schematic diagrams of the interactions (a distance cutoff of 3.8 Å) represent, respectively, the two orientations of the sulfated phytate binding in the standby forms ([A] and [B]); the inhibited form is shown in (C).

cused on the effects exerted by the P loop and the substrate binding pocket. The native enzyme has an activity of 270 unit/mg (see Experimental Procedures, normalized to 100%) in the dephosphorylation of phytate. Mutation of Cys241 in the P loop to alanine completely (down to 0.0%) abolished the enzyme activity, confirming that Cys241 played an essential role as in other PTPs. We also mutated three residues (Tyr298, Tyr138, and His213) that form the substrate binding pocket. Tyr298 directly interacted with the IHS in the inhibited form of the complex, but Tyr138 did not. Mutation of Tyr298 to Phe was shown to reduce the phytase activity by 52%, but mutation of Tyr138 to Phe had no obvious effect on the phytase activity.

The mutation of the important His213 of the WPD loop to alanine decreased the activity of phytase by 94%, suggesting its important role in the inositol polyphosphate binding. This is similar to the role of His93 of the WPD loop in PTEN (Lee et al., 1999). In addition, the mutation of His151 to alanine on helix αC, to which the nonactive site IHS was bound in the crystal, showed no effect on the enzyme activity. This excludes the possibility that His151 is involved in the activity of phytase (Lim et al., 2000).

Insights into Evolution by Structural Comparison

The topology of the large domain of phytase is similar to the conserved domain of the dual-specificity phosphatases KAPt and PTEN (Figures 4A–4C). Comparison of the crystal structures of phytase, PTEN, and KAPt highlights a conserved fold containing a twisted five-stranded β sheet packed against four α helices (αE, αF,

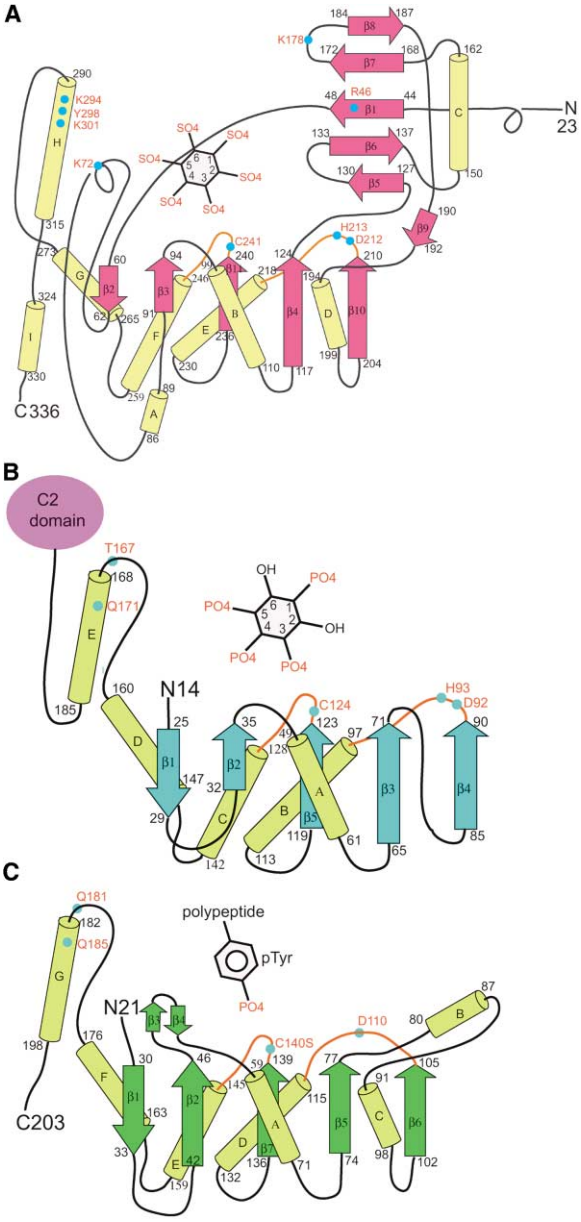

Figure 4. Topology Diagram of the *S. ruminantium* Phytase and Its Comparison with Other Phosphatases

Topology diagram of the *S. ruminantium* phytase (A), PTEN (B), and KAPt (C). The *S. ruminantium* phytase shows clearly that the active site is located at the interface between the two domains, surrounded by several loops (β7-β8 loop, β2-αA loop, conserved P loop, and WPD loop), strand β7, and helix H. The catalytic core of those three phosphatases shares remarkable similarities, having a conserved five-stranded β sheet and five α helices surrounding the active site. Their respective substrate analogs are shown.

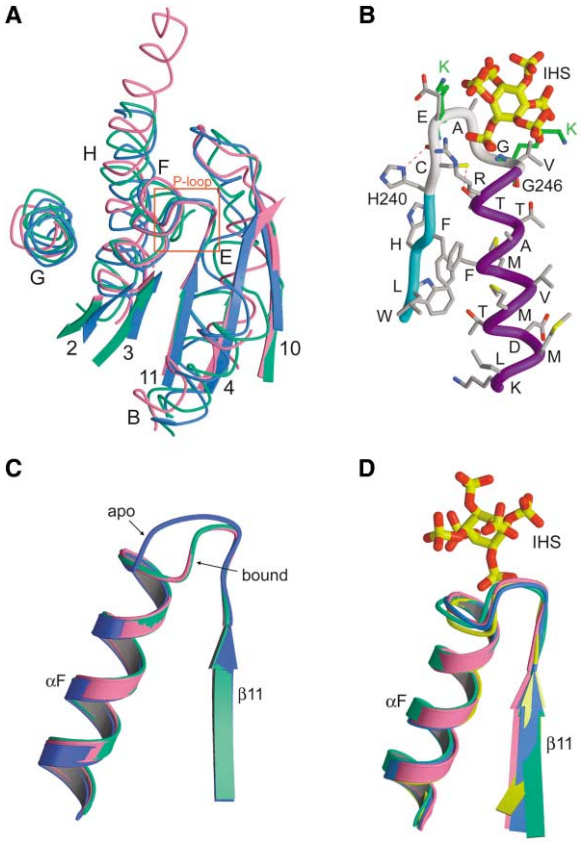

Figure 5. Structural Comparison of the *S. ruminantium* Phytase with Other Phosphatases

(A) A superposition of the *S. ruminantium* phytase (red), PTEN (magenta) (Protein Data Bank [PDB] code 1D5R), and KAPt (green) (PDB code 1FQ1) shows a conserved fold containing five twisted β strands packed against four α helices (αE, αF, αG, and αH) on one side and an α helix (αB) on the other side. The conserved P loop is depicted in a red box.

(B) In the phytase HCXXGXXR(S/T) motif, highly conserved residues His240 and Thr248 are important in terms of the conformation of the P loop and hydrolysis. Gly244 is strictly conserved due to its role in the switch between the apo and substrate-bound conformation. Arg247, another strictly conserved residue, interacts with the negatively charged phosphate of the phytate substrate. Those two lysines (green) in PTEN show the different substrate specificity with *S. ruminantium* phytase.

(C) The P loop of the apo form (blue) adopts a different conformation of residues 240–247 from those of the standby form (green) and inhibited form (magenta).

(D) P loops of *S. ruminantium* phytase, PTEN (PDB code 1D5R), KAPt (PDB code 1FQ1), and PTP1B (PDB code 1PTY) adopt a similar conformation of the bound state.

αG, and αH) on one side and an α helix (αB) on the other side (Figure 5A). The superposition of phytase to PTEN and KAPt using the Cα atoms of the core elements yields rmsd. values of 1.45 Å (416 atoms) and 1.58 Å (364 atoms), respectively. The structures diverge outside of the core region. There are several distinct structural differences, of which the most prominent are as follows. (1) A long extended region (β2 to β3 strand) replaces the β2-β3 loop in PTEN and KAPt. (2) The αH helix of the phytase is 26 amino acid residues longer than the equivalent helix of PTEN and KAPt. (3) A small domain is inserted to the region between the β4 to β10 strand in phytase. Those differences produce a wider and deeper cavity with an highly positively charged surface in phytase. These divergent areas are the key components for the phytase to preferentially bind to its substrate, phytate.

A structure-based amino acid sequence alignment shows that the conserved residues, HCXXGXXR(T/S), are located in the P loop, and the residues interacting

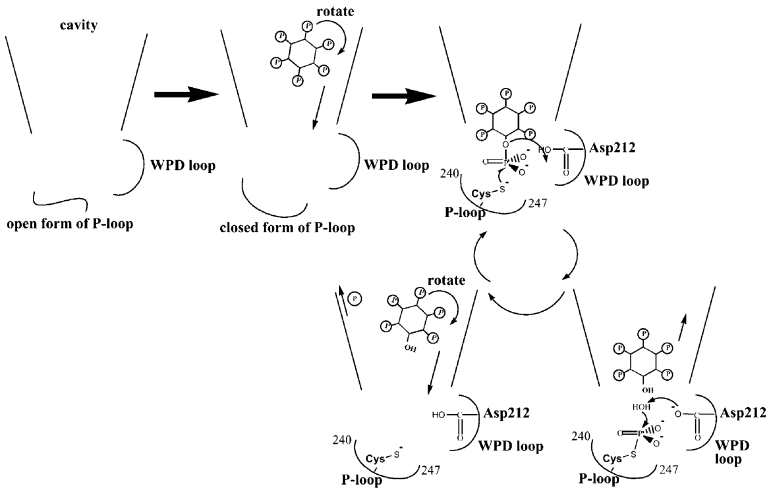

Figure 6. The Proposed Catalytic Mechanism for *S. ruminantium* Phytase

Once the inhibitor moves nearby the cavity of phytase, the conformation of the phytase changes from the apo form to the standby form, and the P loop changes its conformation from open form to closed form. Next, the inhibitor contacts the P loop to generate the inhibited form. In addition, keeping the closed conformation of the P loop favors a mechanism of sequential dephosphorylation of phytase.

with inhibitor are colored yellow (Figure 1A). The His240 and Gly244 residues in the HCXXGXXR motif are important in the conformation of the P loop, like those in the PTP1B-substrate complex (Zhang, 2002). Gly244 is a key residue in the switch between the open and closed conformations of the P loop in the apo and inhibited forms, respectively (Figures 5B and 5C). His240 forms a hydrogen bond with the carbonyl group of the cysteine residue in the P loop, like that in Yersinia PTP (Stuckey et al., 1994). The Sγ of Cys241 is also within hydrogen bond distance of Oδ of Thr248 (found to be conserved as threonine or serine in other cysteine phosphatases). These interactions associated with the P loop were also found in PTEN, KAPt, and PTP1B (Figure 5D) and are believed to help maintain the P loop in a catalytically competent conformation.

PTEN and TPIP are two related PTP-like proteins, which contain two lysine residues in the P loop (Lee et al., 1999). These observations are different from other PTP enzymes. These two lysines are important for PTEN activity against PtdIns(3,4,5)P(3). The structure of the inhibited form of the phytase shows that the P loop adopts a closed form and brings the side chain of Val245 in contact with the 3-sulfate group of inhibitor. Therefore, Lys128 of PTEN (equivalent to Val245 of our phytase) and Lys125 may interact with the phosphate groups of its substrate and increase the substrate specificity (Figure 5B).

The conserved Asp212-His213 pair in the WPD loop has been identified in several PTP-like proteins with phosphoinositide phosphatase activity, such as PTEN, TPIP, and myotubularin (Lee et al., 1999; Walker et al., 2001; Taylor et al., 2000). In our structure of the phytase-inhibitor complex, His213 is in close proximity to the S4 and S6 sulfate groups (Figure 2D).

Taken together, these observations suggest that many basic groups surrounding the active-site pocket of phytase along with the strong interactions between His213 and (sulfated) phytate allow the phytase to have high specificity toward the substrate, and the enzyme-specific interactions of the PTP family are evolutionally conserved.

Implications for Phytase Function

Phytase catalyzes dephosphorylation of phytate from *myo*-inositol hexakisphosphate to monophosphate. Furthermore, phytase, unlike PTEN, PTPRQ (Oganesian et al., 2003), and myotubularin (Taylor et al., 2000), which have both activities of protein tyrosine phosphatase and phosphoinositide phosphatase, shows no activity toward a widely used PTP substrate *para*-nitrophenylphosphate (pNPP). The pNPP substrate contains a hydrophobic aromatic ring, unfavorable for interactions with the basic charges surrounding the active-site pocket of phytase. Thus, our phytase has the dual-specificity protein phosphatase fold and a specific activity for *myo*-inositol polyphosphate. Although the folding and catalytic mechanism of our phytase are significantly different from *E. coli* or *B. amyloliquefaciens*, all of them generate a favorable electrostatic potential using certain Lys and Arg residues for the substrate binding.

Based on the well-studied mechanism of the classical dual-specificity phosphatase and the three different structures from three crystal forms, we proposed a catalytic reaction to proceed through the following steps (Figure 6). First, the initial binding of phytate to the active-site pocket is mainly facilitated by the interactions between the basic charges in the pocket and the negatively charged groups on phytate. This binding is advantageous to increase the possibility of a continuous dephosphorylation reaction. The phytate is then oriented to the productive position by hydrogen bonds between its phosphate group and amide NH groups of amino acids 242–247 of the P loop of the phytase. The thiolate anion of Cys241 attacks the position 5 phosphate of phytate and forms a cysteinyl-phosphate trigonal-bipyrimidal pentavalent intermediate.

Dixon et al. (Denu and Dixon, 1995) suggested that the negative charge on the Sγ atom of Cys241 is stabilized by a hydrogen bond to the hydroxyl group of Ser/Thr residue within the P loop. In our structure, the distance of the hydroxyl group of Thr248 to the Sγ atom of Cys241 is 3.32 Å, consistent with Dixon's suggestion. Release of *myo*-inositol pentakisphosphate follows the donation of a proton by Asp212, acting as a general

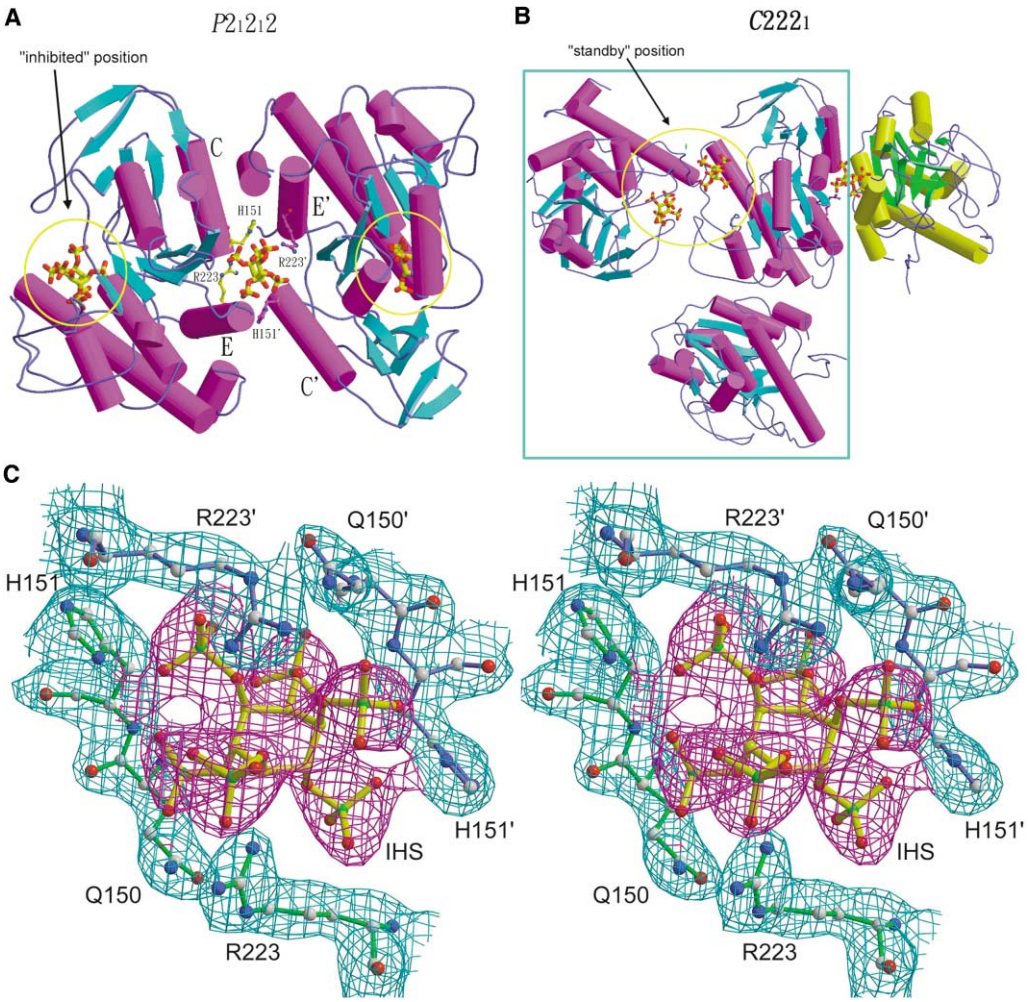

Figure 7. Crystal Packing and Sulfated Phytate Conformation

(A) Two independent phytases in the asymmetric unit of *P*2,2,2 crystal form are drawn together to become a "dimer" mediated by an IHS molecule. Each phytase has an IHS bound at the active site in the inhibited position.

(B) Three phytase molecules (magenta) are found in the asymmetric unit of the $C222_1$ form. Two of the three phytase enzymes have the IHS inhibitor bound at the standby position due to the interactions between IHS and the neighboring phytase. The third phytase has no inhibitor at the active site, but is linked to the neighboring phytase through an IHS inhibitor.

(C) A stereo view of 2.0 Å $2F_o - F_c$ electron density map contoured at 1σ level. All sulfated phytates in the present crystal forms adopt a 5-axial/1-equatorial conformation.

acid and stabilized by Asp142. For the second step of the catalytic reaction, the same aspartate acts as a general base to take a proton from the water molecule bound to Lys301 and, in turn, attacks the phosphor-enzyme intermediate to eliminate the phosphate and regenerate the active phytase. In further sequential reactions, pentakisphosphate inositide in the standby site reorients and rebinds to the active site, proceeding with the next hydrolysis cycle. Finally, the end product is inositol 2-monophosphate.

The proposed mechanism implies significant reorientation of the substrate in the active-site pocket without its release into solution, as well as specific binding of the same substrate in two distinct orientations. In order to perform this rotation without causing significant steric clashes in the active site, the intermediate must first dissociate from its high-affinity binding site, diffuse into the larger active site cleft, rotate, and then rebind in different orientation. Electrostatic interactions between the positively charged active site and the substrate/intermediate of phytase may provide sufficient nondirectional binding energy to allow the reorientation of the intermediate without dissociation from the active site.

In conclusion, *S. ruminantium* phytase possesses a catalytic P loop motif similar to those found in protein tyrosine/dual-specificity phosphatases (Nam et al., 1999), metazoan RNA triphosphatase (Song et al., 2001), and phosphoinositide phosphatase (Lee et al., 1999). This finding has led us to the prediction of structural and mechanistic conservation between phytase and other members of the cysteine phosphatase superfamily. The crystal structure of the phytase and structure-based mutational analyses reveal that the structure of phytase is most similar to phosphoinositide phosphatases and

highlight unique features of the catalytic mechanism of phosphoinositide phosphatases.

Experimental Procedures

Sample Preparation and Crystallization

The *S. ruminantium* phytase (343 amino acids) gene (GeneBank AF177214) was cloned into the pET23b (Novagen) vector and overexpressed in *Escherichia coli* BL21 (DE3) (Novagen). Se-Met phytase was prepared according to the protocols described previously (Guerrero et al., 2001). Both proteins were purified from Ni-NTA column with 25 mM Tris (pH 7.5), 150 mM NaCl, and 300 mM imidazole and concentrated to 10 ml by Amicon (Millipore). Proteins were lyophilized and stocked after salt removal by HiPrep 26/10 desalting column (Amersham Biosciences). Mutant proteins of H151A, C241A, H213A, Y298F, and Y138F were prepared by using QuikChange Site-Directed Mutagenesis Kit (Stratagene) according to the manufacturer's instructions. For the crystallization experiment, the phytase and Se-Met phytase proteins were dissolved in deionized water to make a 10 mg/ml stock solution. The hanging-drop vapor diffusion method was used, with the protein-to-reservoir ratio being 1 μl:1 μl. With Hampton Research crystallization kits for the initial screening, we obtained crystals of Se-Met phytase (apo form) with 0.1 M sodium chloride, 0.1 M sodium acetate trihydrate (pH 4.6), and 12% PEG 6000. Cocrystals of phytase with *myo*-inositol hexasulfate (inhibited form) were obtained using the reservoir containing 0.1 M Tris-HCl (pH 7.5), 20 mM $Ca(OAc)_2$, and 10% PEG8000. Cocrystals of Se-Met phytase with the same compound (standby form) were obtained with the reservoir containing 0.1 M LiCl, 0.05 M CAPSO (pH 9.0), 12% PEG6000, and 2% PEG200. The reservoir volume was 500 μl. Crystals were soaked overnight in a cryoprotectant containing 30% glycerol.

Data Collection and Structure Determination

We collected the selenium single-wavelength anomalous diffraction data of the enzyme and its complex with *myo*-inositol hexasulfate at Taiwan beamline BL12B2 in SPring-8, Japan. The ADSC Quantum 4R charge-coupled device and Oxford Cryostream cooler were used for data collection. Data for the native phytase complex with *myo*-inositol hexasulfate were collected with a Rigaku R-Axis IV^{2+} image plate at the BL17B2 beamline in the National Synchrotron Radiation Research Center, Hsinchu, Taiwan. The data were processed and integrated with DENZO and SCALEPACK (Otwinowski and Minor, 1997). The detailed statistics are listed in Table 1. The structure of *S. ruminantium* phytase was determined by the single-wavelength anomalous diffraction method using data collected at the L_{III} peak (λ = 0.9797 Å) of Se and was phased by SOLVE (Terwilliger and Berendzen, 1999) with the data 25 to 2.8 Å range. Further density modification, model building, and refinement were done with RESOLVE (Terwilliger, 2001), XtalView (McRee, 1999), and the CNS program (Brünger et al., 1998). Improvement of the model was guided by the sigma A-weighted $2F_o - F_c$ electron density maps. Amino acids 1–22, 337–343 of the inhibited form of phytase were not visible in the electron density maps and were presumed to be disordered.

Phytases in Three Crystal Lattices

Three distinct crystal forms of space groups $P2_1$, $P2_12_12$, and $C222_1$ were crystallized from different crystallization conditions (see Experimental Procedures). In the $P2_1$ form (apo form), which has no IHS binding to the enzyme, each enzyme molecule in the asymmetric unit is connected to the symmetry related enzyme by a local dyad axis. Their contact surface area involves the β2-αA and the αG-αH loops. Crystals of both the $P2_12_12$ (inhibited) and $C222_1$ (standby) forms were grown in the presence of sulfated phytates. In the $P2_12_12$ form, there are two phytase and three sulfated-phytate molecules in the asymmetric unit. As shown in Figure 7A, an IHS is visible at the interface between two phytase molecules related by a local dyad axis. The sulfated phytate at the interface interacts with side chain atoms of Gln150, His151, and Arg223 of each phytase. Moreover, each phytase has an IHS molecule occupied in its active site to form the inhibited form of the complex.

The asymmetric unit contains three phytase molecules and three sulfated phytates in the $C222_1$ form (Figure 7B). Interestingly, only two phytases are bound with IHS, but the third enzyme is an apo form without a bound inhibitor. The bound sulfated phytate, surrounded by a positively charged region slightly away from the active site, further interacts with a noncrystallographic dyad-related phytase involving the β2-αA loop and the αG-αH loop. A dimer in the $C222_1$ form was created by two symmetry related phytase molecules using a crystallographic two-fold axis with the third IHS molecule being at the interface. This assembly is different from the dimer in the $P2_12_12$ form.

In all, there are seven independent phytase molecules from three crystal forms. The conformations are generally similar, with the rmsd values among the seven molecules ranging between 0.27 to 0.67 Å (using 312 Cα atoms), with an average value of 0.56 Å. Some differences are observed in regions that are involved in inhibitor binding (e.g., P loop) or in crystal packings. The apo and the standby form of the phytase were grown in pH 4.6 and pH 9.0, respectively. The large pH shift not only affected the conformations but also the surface charge potential. Those changes could determine the way surface-charged amino acids interact at the crystal contacts of neighboring phytases.

All six IHS molecules found in the three crystal forms have their phosphates arranged in the 5-axial/1-equatorial conformation (Figure 7C), different from the 5-equatorial/1-axial conformation of the phytate bound to *E. coli* phytase. The 5-axial/1-equatorial conformation is also observed in deoxyhemoglobin-phytate complex (Arnone and Perutz, 1974). Our observation here may suggest that the 5-axial/1-equatorial conformation is the lowest energy form.

Phytase Assays

Phytase activity of the cell-free supernatant was measured for each isolate (Bae et al., 1999). All reactions were done in triplicate. The vector controls showed no phytase activity. Results were compared to a standard curve prepared with inorganic phosphate (KH_2PO_4). The substrate solution (0.6 ml) (0.2% [w/v] sodium phytate [Sigma, St Louis, MO] in 0.1 M sodium acetate buffer [pH 5.0]) and the sample solution (0.075 ml) (culture filtrates, cell suspensions, lysates, washes, or distilled water blanks) were mixed together in a tube. The mixture was incubated for 30 min (incubation time depends upon activity of sample) at 37°C. Then, 0.75 ml of 5% TCA was added to stop the reaction. Finally, 0.75 ml of coloring solution was added to react with the free phosphate. The color reagent was prepared by mixing four volumes of 1.5% (w/v) ammonium molybdate in a 5.5% (v/v) sulfuric acid solution, and one volume of a 2.7% (w/v) ferrous sulfate solution was added to the sample solution. The production of phosphomolybdate was measured spectrophotometrically at 700 nm. Phytase activity was measured as the amount of inorganic phosphate released, and sodium phytate (0.2% w/v) was used as the substrate in 0.1 M sodium acetate buffer (pH 5.0), with 30 min incubation at 39°C (Shimizu, 1992). One unit (U) of phytase was defined as the amount of enzyme required to liberate one nanomole P*i* per minute under the given assay conditions.

Acknowledgments

The synchrotron data collections were conducted with the Biological Crystallography Facilities (Beamline BL17B2 at NSRRC in HsinChu, Taiwan and Taiwan Beamline BL12B2 at SPring-8, Japan) supported by the National Science Council (NSC). This work was supported by the Academia Sinica and the National Science Council (NSC91-3112-P-001-019-Y) to A.H.-J.W.

Received: May 28, 2004
Revised: August 23, 2004
Accepted: August 24, 2004
Published: November 9, 2004

References

Arnone, A., and Perutz, M.F. (1974). Structure of inositol hexaphosphate–human deoxyhaemoglobin complex. Nature *249*, 34–36.

Bae, H.D., Yanke, L.J., Cheng, K.J., and Selinger, L.B. (1999). A

novel staining method for detecting phytase activity. J. Microbiol. Methods *39*, 17–22.

Brünger, A.T., Adams, P.D., Clore, G.M., DeLano, W.L., Gros, P., Grosse-Kunstleve, R.W., Jiang, J.S., Kuszewski, J., Nilges, M., Pannu, N.S., et al. (1998). Crystallography & NMR system: a new software suite for macromolecular structure determination. Acta Crystallogr. D Biol. Crystallogr. *54*, 905–921.

Caffrey, J.J., Hidaka, K., Matsuda, M., Hirata, M., and Shears, S.B. (1999). The human and rat forms of multiple inositol polyphosphate phosphatase: functional homology with a histidine acid phosphatase up-regulated during endochondral ossification. FEBS Lett. *442*, 99–104.

Changela, A., Ho, C.K., Martins, A., Shuman, S., and Mondragon, A. (2001). Structure and mechanism of the RNA triphosphatase component of mammalian mRNA capping enzyme. EMBO J. *20*, 2575–2586.

Denu, J.M., and Dixon, J.E. (1995). A catalytic mechanism for the dual-specific phosphatases. Proc. Natl. Acad. Sci. USA *92*, 5910–5914.

Denu, J.M., and Dixon, J.E. (1998). Protein tyrosine phosphatases: mechanisms of catalysis and regulation. Curr. Opin. Chem. Biol. *2*, 633–641.

Denu, J.M., Lohse, D.L., Vijayalakshmi, J., Saper, M.A., and Dixon, J.E. (1996). Visualization of intermediate and transition-state structures in protein-tyrosine phosphatase catalysis. Proc. Natl. Acad. Sci. USA *93*, 2493–2498.

Guerrero, S.A., Hecht, H.J., Hofmann, B., Biebl, H., and Singh, M. (2001). Production of selenomethionine-labelled proteins using simplified culture conditions and generally applicable host/vector systems. Appl. Microbiol. Biotechnol. *56*, 718–723.

Guex, N., and Peitsch, M.C. (1997). SWISS-MODEL and the Swiss-PdbViewer: an environment for comparative protein modeling. Electrophoresis *18*, 2714–2723.

Guipponi, M., Tapparel, C., Jousson, O., Scamuffa, N., Mas, C., Rossier, C., Hutter, P., Meda, P., Lyle, R., Reymond, A., et al. (2001). The murine orthologue of the Golgi-localized TPTE protein provides clues to the evolutionary history of the human TPTE gene family. Hum. Genet. *109*, 569–575.

Ha, N.C., Oh, B.C., Shin, S., Kim, H.J., Oh, T.K., Kim, Y.O., Choi, K.Y., and Oh, B.H. (2000). Crystal structures of a novel, thermostable phytase in partially and fully calcium-loaded states. Nat. Struct. Biol. *7*, 147–153.

Holm, L., and Sander, C. (1998). Touring protein fold space with Dali/FSSP. Nucleic Acids Res. *26*, 316–319.

Hoy, M., Efanov, A.M., Bertorello, A.M., Zaitsev, S.V., Olsen, H.L., Bokvist, K., Leibiger, B., Leibiger, I.B., Zwiller, J., Berggren, P.O., and Gromada, J. (2002). Inositol hexakisphosphate promotes dynamin I-mediated endocytosis. Proc. Natl. Acad. Sci. USA *99*, 6773–6777.

Kim, J.H., Shin, D.Y., Han, M.H., and Choi, M.U. (2001). Mutational and kinetic evaluation of conserved His-123 in dual specificity protein-tyrosine phosphatase vaccinia H1-related phosphatase. J. Biol. Chem. *276*, 27568–2754.

Kostrewa, D., Gruninger-Leitch, F., D'Arcy, A., Broger, C., Mitchell, D., and van Loon, A.P. (1997). Crystal structure of phytase from Aspergillus ficuum at 2.5 Å resolution. Nat. Struct. Biol. *4*, 185–190.

Lee, J.O., Yang, H., Georgescu, M.M., Di Cristofano, A., Maehama, T., Shi, Y., Dixon, J.E., Pandolfi, P., and Pavletich, N.P. (1999). Crystal structure of the PTEN tumor suppressor: implications for its phosphoinositide phosphatase activity and membrane association. Cell *99*, 323–334.

Lim, D., Golovan, S., Forsberg, C.W., and Jia, Z. (2000). Crystal structures of Escherichia coli phytase and its complex with phytate. Nat. Struct. Biol. *7*, 108–113.

Liu, B.L., Rafiq, A., Tzeng, Y.M., and Rob, A. (1998). The induction and characterisation of phytase and beyond—a review. Enzyme Microb. Technol. *22*, 415–424.

Lohse, D.L., Denu, J.M., Santoro, N., and Dixon, J.E. (1997). Roles of aspartic acid-181 and serine-222 in intermediate formation and hydrolysis of the mammalian protein-tyrosine-phosphatase PTP1. Biochemistry *36*, 4568–4575.

McRee, D.E. (1999). XtalView/Xfit—a versatile program for manipulating atomic coordinates and electron density. J. Struct. Biol. *125*, 156–165.

Michell, R.H. (2002). Inositol phosphates: a remarkably versatile enzyme. Curr. Biol. *12*, R313–R315.

Mitchell, C.A., Gurung, R., Kong, A.M., Dyson, J.M., Tan, A., and Ooms, L.M. (2002). The structure and function of catalytic domains within inositol polyphosphate 5-phosphatases. IUBMB Life *53*, 25–36.

Nam, H.J., Poy, F., Krueger, N.X., Saito, H., and Frederick, C.A. (1999). Crystal structure of the tandem phosphatase domains of RPTP LAR. Cell *97*, 449–457.

Nicholls, A., Sharp, K., and Honig, B. (1991). Protein folding and association: insights from the interfacial and thermodynamic properties of hydrocarbons. Proteins *11*, 281–296.

Oganesian, A., Poot, M., Daum, G., Coats, S.A., Wright, M.B., Seifert, R.A., and Bowen-Pope, D.F. (2003). Protein tyrosine phosphatase RQ is phosphatidylinositol phosphatase that can regulate cell survival and proliferation. Proc. Natl. Acad. Sci. USA *100*, 7563–7568.

Otwinowski, Z., and Minor, W. (1997). Processing of X-ray diffraction data collected in oscillation mode: Macromolecular crystallography Part A. Methods Enzymol. *276*, 307–326.

Shamsuddin, A.M. (1999). Metabolism and cellular functions of IP6: a review. Anticancer Res. *19*, 3733–3736.

Shimizu, M. (1992). Purification and characterization of phytase from *Bacillus subtilis*. Biosci. Biotech. Biochem. *56*, 1266–1269.

Song, H., Hanlon, N., Brown, N.R., Noble, M.E.M., Johnson, L.N., and Barford, D. (2001). Phosphoprotein—protein interactions revealed by the crystal structure of kinase-associated phosphatase in complex with pohosphoCDK2. Mol. Cell *7*, 615–616.

Streb, H., Irvine, R.F., Berridge, M.J., and Schulz, I. (1983). Release of Ca^{2+} from a nonmitochondrial intracellular store in pancreatic acinar cells by inositol-1,4,5-trisphosphate. Nature *306*, 67–69.

Stuckey, J.A., Schubert, H.L., Fauman, E.B., Zhang, Z.Y., Dixon, J.E., and Saper, M.A. (1994). Crystal structure of Yersinia protein tyrosine phosphatase at 2.5 Å and the complex with tungstate. Nature *370*, 571–575.

Taylor, G.S., Maehama, T., and Dixon, J.E. (2000). Inaugural article: myotubularin, a protein tyrosine phosphatase mutated in myotubular myopathy, dephosphorylates the lipid second messenger, phosphatidylinositol 3-phosphate. Proc. Natl. Acad. Sci. USA *97*, 8910–8915.

Terwilliger, T.C. (2001). Map-likelihood phasing. Acta Crystallogr. D Biol. Crystallogr. *57*, 1763–1775.

Terwilliger, T.C., and Berendzen, J. (1999). Automated MAD and MIR structure solution. Acta Crystallogr. D Biol. Crystallogr. *55*, 849–861.

Walker, S.M., Downes, C.P., and Leslie, N.R. (2001). TPIP: a novel phosphoinositide 3-phosphatase. Biochem. J. *360*, 277–283.

Yanke, L.J., Selinger, L.B., and Cheng, K.J. (1999). Phytase activity of Selenomonas ruminantium: a preliminary characterization. Lett. Appl. Microbiol. *29*, 20–25.

York, J.D., Ponder, J.W., Chen, Z.W., Mathews, F.S., and Majerus, P.W. (1994). Crystal structure of inositol polyphosphate 1-phosphatase at 2.3 Å resolution. Biochemistry *33*, 13164–13171.

Zhang, Z.Y. (2002). Protein tyrosine phosphatases: structure and function, substrate specificity, and inhibitor development. Annu. Rev. Pharmacol. Toxicol. *42*, 209–234.

Accession Numbers

The structure factors and atomic coordinates reported in this paper have been deposited in the Protein Data Bank with ID codes 1U24, 1U25, and 1U26.